CERN-ACC-2020-0001
13-01-2020
androula.alekou@cern.ch

Report

Deliverable 2.7: Analysis of the existing sources of blow-up in the SPS by experiments and estimation/measurement of the effect of the crab cavities in the SPS

A. Alekou[1, 2], F. Antoniou[1], R. B. Appleby[2], H. Bartosik[1], R. Calaga[1], M. Carla[1], L. Carver[*1, 3], Y. Papaphilippou[1], C. Welsch[3]*
[1]CERN, Switzerland, [2]University of Manchester and Cockcroft Institute, [3]University of Liverpool

Abstract

The Crab Cavities (CCs) may induce emittance growth, driven by phase and amplitude jitter, and lead to a degradation of the High Luminosity LHC (HL-LHC) beam. Furthermore, the tight HL-LHC space constraints call for non-axially symmetric cavity designs that come with higher order non-linearities which can affect the long-term dynamic aperture (DA). In order to study the effect the CCs have on the beam and the engineering challenges to validate the pre-series design, a prototype HL-LHC CC set was installed in the SPS machine in the year-end technical stop (YETS) of 2017-2018, and the first ever CC tests with protons were performed in 2018. This note is a collection of the reports and work done on the emittance growth measurements prior [1–4] and after [5] the CC installation, as well as simulations [6] and measurements [7] performed to study the CC and SPS nonlinearities effect. Finally, a summary of the instrumentation observations of the SPS CC experimental measurements [8] is presented.

Keywords: Crab Cavities, HL-LHC, SPS, emittance growth, Dynamic Aperture.

[*]Now at ESRF, Grenoble, France.

Contents

1 Emittance growth in the SPS

One of the most important concerns that needed to be addressed during the SPS CC experiments of 2018 was the induced emittance growth driven by the CC phase and amplitude jitter. A theoretical emittance growth model has been developed [5] that takes into account the natural emittance growth of the SPS machine, i.e. the growth present without the CCs, and the induced growth. To better benchmark this theoretical model several experimental studies were performed from 2010 to 2016 in the absence of CCs aiming to characterise the natural emittance growth for different beam and machine parameters [1–4] and distinguish it from the CC noise that was studied during the SPS experiments in the presence of CCs [5].

1.1 Before the CC installation

Several machine development (MD) studies (experimental sessions) were devoted in the past years to the study of the natural long-term emittance growth in the SPS. Special cycles with a constant beam energy, called "coast" beam cycles, were set-up with single very low intensity bunches ($\sim 10^{10}$ p/b).

During the experimental sessions of 2010-2015 three different energies were studied, the results of which can be found in [1]. The conclusion was that the SPS transverse emittance growth is primarily a single bunch effect that is more important in lower than higher energies. The transverse tune working point effect was minimal when using very low intensity bunches (10^{10} ppb), even in the proximity of the 3^{rd} order resonance, whereas the chromaticity had a strong effect; the emittance growth was found to be almost proportional to Q'. Up until 2012 the horizontal and vertical emittances had similar growth slopes; however a different behaviour was observed in 2015. The October 2015 results, presented in Fig. 1, show a significantly larger horizontal growth than the vertical one. A similar trend was also observed in the May 2015 MD.

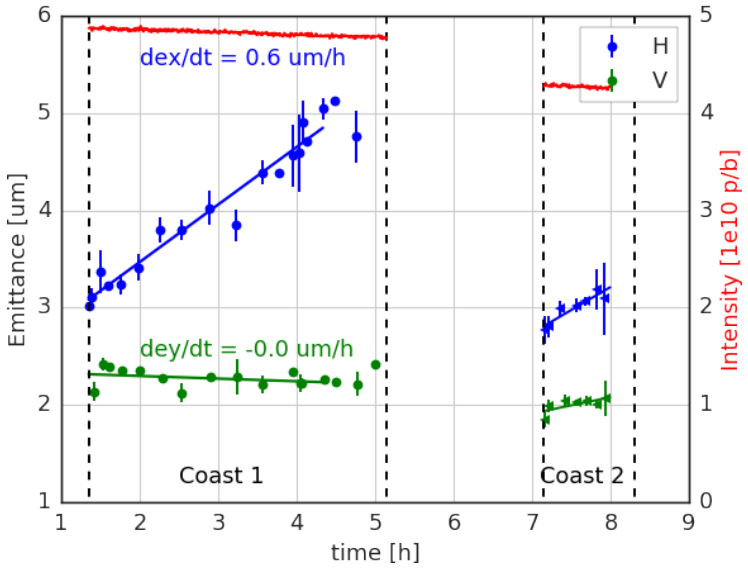

Fig. 1: Emittance growth studies in coast beam in the SPS at 270 GeV, in 2015.

The MDs that took place from 2016 to 2017 were performed with single bunches at 270 GeV, mainly with low intensity (1-4·10^{10} ppb). The effect of additional parameters in both transverse and longitudinal planes were also studied.

1.1.1 Off-bucket losses

Slow off-bucket losses were observed for all single bunch, low intensity MDs up to 2016. The effect of the RF voltage and low level RF loops on the losses were investigated in the SPS Coast MD of 10 May 2017, at 270 GeV, where the RF voltage was scanned ($Q_{x,y}$=26.13, 26.18, Q' ~1 in both planes). It was found that the RF voltage had no impact on the losses, however a clear correlation between the RF feedback and the losses was observed. The total beam (red) and bunch (blue) intensities are shown in

Fig. 2 as measured by the DC and fast beam current transformer (BCT) respectively. The RF feedback, which was initially on, was switched off after 1 h (brown vertical line). As can be seen, while the RF feedback was on there was a clear deviation between the total beam and bunch intensities, something that indicates slow off-bucket losses. Once the RF feedback was switched off the two slopes became similar. Following this observation, all coast experiments with single bunches and low intensities were performed without the RF feedback. It is believed that the losses occurred because the role of the RF feedback is to kill the instabilities produced by intensity effects in nominal high intensity beams (10^{11} ppb), therefore when using low intensity beams the effect the feedback had instead resulted in noise introduction.

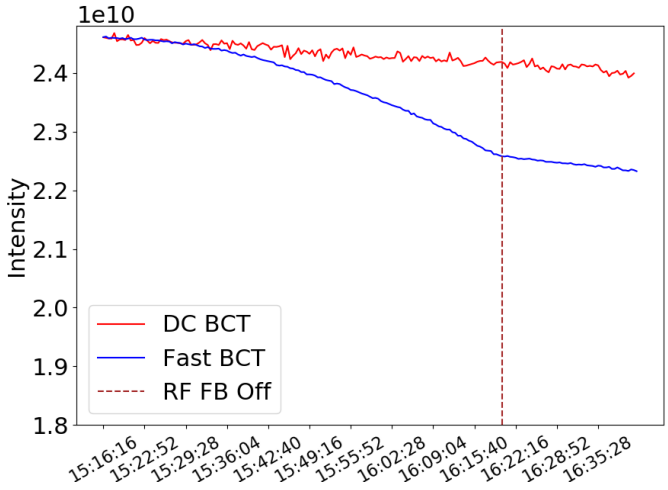

Fig. 2: Time evolution of the total intensity from DC-BCT (red) and bunch intensity from the fast BCT (blue). The RF feedback is switched off after 1 h in coast (brown-dashed) citefanou1.

1.1.2 Chromaticity

The last MD of 2016 was dedicated to the study of the chromaticity impact on the transverse emittance (see Table 1 for beam and machine parameters). A first coast (Coast 1) was injected with a single bunch intensity of $4.25{\cdot}10^{10}$ ppb. The Q' of the machine was corrected to 0.5 and 1 in the horizontal and vertical planes respectively (for lower chromaticity values the beam motion becomes unstable). After 1.8 hours in Coast 1, the beam was dumped and a fresh beam was injected (Coast 2), with the same chromaticity values but with a lower bunch intensity of $1.65{\cdot}10^{10}$ ppb. The bunch evolution was recorded for 2.5 h under the same conditions while later, in the same coast, the chromaticity was increased by 2 units in both planes. Figure 3 (left) shows the time evolution of the horizontal (blue) and vertical (green) emittances during the MD. A linear fit was applied for the three different tests: (1) Coast 1, (2) Coast 2 with reduced intensity and (3) Coast 2 after the chromaticity change. Comparing the fit results it becomes clear that reducing the intensity resulted in a small increase of the horizontal emittance growth and had no impact on the vertical emittance growth; this was also observed in the 2012-2016 MDs. After the chromaticity increase, a clear slope increase was observed, especially in the horizontal plane.

An additional MD took place that also measured the emittance growth as a function of chromaticity. Unlike previous studies [1], there was no observed correlation with the chromaticity (see Fig. 3, right). Furthermore, the emittance growth in the vertical plane was found to be 2-3 times smaller than in all previous MDs. The two main differences between this MD and the previous ones, that could result in this change of the chromaticity effect were: a) the transverse beam profiles during this MD were more Gaussian, and b) this MD took place after the LHC shutdown and the current to all extraction elements (kickers and septa) was set to zero.

Note that during Coast 2, after the chromaticity change, multiple wire-scan measurements were performed (see purple vertical line in Fig. 3) to see if the interaction between the wire and the beam leads to emittance growth [9]. A slight increase in the vertical emittance growth slope was observed but the effect was considered negligible for the performed number of scans. Note that the wire scanners

used were the rotational type that have a higher speed compared to the linear ones (15 m/s compared to 10 m/s respectively), and the higher speed has a smaller effect on the multipole Coulomb scattering. No conclusive results were obtained as the time interval of those measurements was small and the data spread was large.

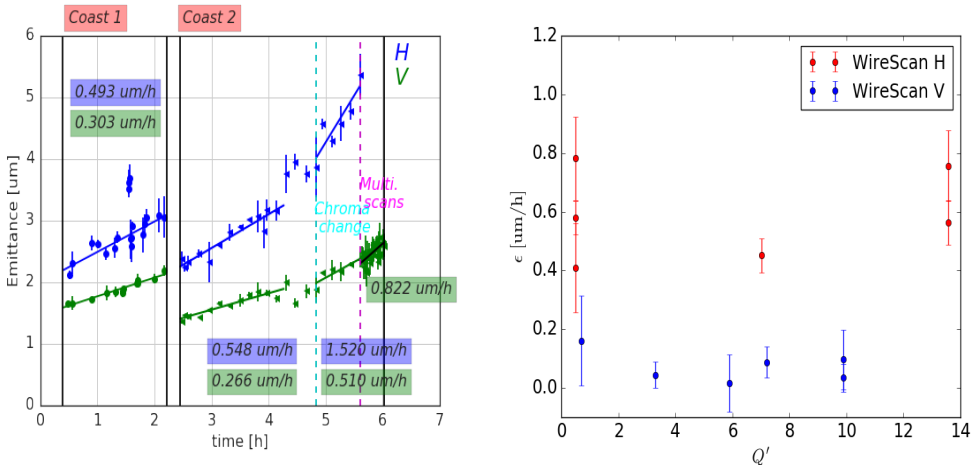

Fig. 3: Left: Horizontal (blue) and vertical (green) emittance evolution. A clear slope increase is observed after the chromaticity increase by 2 units (cyan dashed line). Right: Horizontal (red) and vertical (blue) emittance growth as a function of chromaticity.

1.1.3 Effect of the intra-beam scattering

The intra-beam scattering (IBS) is a multiple Coulomb scattering effect in small angles that can lead, through diffusion, to transverse and longitudinal emittance growth. In the case of zero vertical dispersion, like in the SPS, no effect is expected in the vertical plane [10]. The expected emittance growth due to IBS was estimated for all coasts using the IBS module of MAD-X [11]. The initial bunch characteristics (transverse and longitudinal emittances, and bunch intensity) from the measurements were used as input for each case. Even though IBS can explain part of the observed growth, a residual component on top of it was observed that was very similar between the horizontal and vertical planes. If we assume that the vertical emittance growth is caused by an effect which also acts in the horizontal plane in the same way and convolution this with the IBS effect, the measurement in the horizontal plane can be reproduced very well. This is shown in Fig. 4 and the same observation is valid in all acquired datasets.

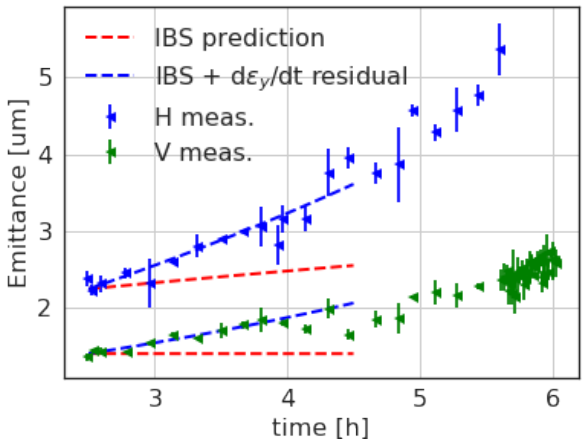

Fig. 4: Intrabeam scattering predictions (red dashed lines) can explain only part of the emittance growth. The residual component is similar in both horizontal and vertical planes. Data and plot from December 2016 MD.

Table 1: Summary results from the MDs of 2016-2017 at 270 GeV

MD	ϵ_x/ϵ_y [μm rad]	N_b [10^{10}]	Optics -	Q'_x/Q'_y -	V_{RF} [MV]	$4\sigma_l$ [ns]	$d\epsilon_x/dt$ [μm/h]	$d\epsilon_y/dt$ [μm/h]
July 2016	2.85/2.16	2.25	"Q26"	2.5/2.5	5.1	1.96	0.59	0.23
Dec. 2016: 1	2.23/1.61	4.25	"Q26"	0.5/1.0	2	2.28	0.49	0.30
Dec. 2016: 2	2.25/1.41	1.65	"Q26"	0.5/1.0	2	2.3	0.55	0.27
Dec. 2016: 3	4.0/1.98	1.65	"Q26"	2.5/3.0	2	-	1.52	0.51
May 2017	Studies of off-bucket losses							
Jun. 2017	2.1/1.7	2.5	"Q26"	1.0/1.6	5	1.9	0.67	0.37
Jul. 2017: 1	7.3/4.8	2.2	"Q20"	0.7/1.4	5	1.7	0.33	0.4
Jul. 2017: 2	2.5/2.0	2.2	"Q20"	0.7/1.4	5	2.0	0.45	0.5
Aug. 2017: 1	1.7/1.4	12	"Q26"	-	-	-	2.71	0.31
Aug. 2017: 2	1.6/1.3	11	"Q26"	-	-	-	1.84	0.48

While the emittance growth measurements studies in 2017 were mostly performed with the "Q26" optics (corresponding to an integer tune of 26), one of the experiments was performed using the "Q20" optics (integer tune of 20) [12], to study the impact of the different optics on the residual growth. Two Q20 coast configurations were used: the first one with a similar expected IBS effect as in the December 2016 MD that used the Q26 optics, and the second one with a reduced IBS effect (see table 1). The expected IBS growth of the Q26 December 2016 MD was found to be 0.36 μm/h, whereas in the Q20 optics it was found to be 0.13 μm/h and 0.3 μm/h in the first and second coasts respectively. In the Q20 optics experiments the residual emittance growth was in both cases of the order of 0.3-0.5 μm/h in both planes, as in the Q26 observations. Parasitic transverse emittance measurements were also acquired with nominal intensity ($1.1{\cdot}10^{11}$ ppb) with an increased IBS effect. The residual growth was also similar in both horizontal and vertical planes and were of the order of 0.3-0.5μm/h.

1.1.4 Other sources of emittance growth

A summary of all the MDs performed in 2016-2017 is shown in Table 1. The vertical emittance growth shows no strong dependence on the chromaticity, the machine optics or the bunch intensity. Part of the horizontal emittance growth can be explained by IBS while the residual growth appears to be similar in the two transverse planes, varying from 0.3-0.5μm/h. This gives an indication that the vertical emittance growth is dominated by some other noise mechanisms. The effects of power supply ripple and residual gas scattering were investigated.

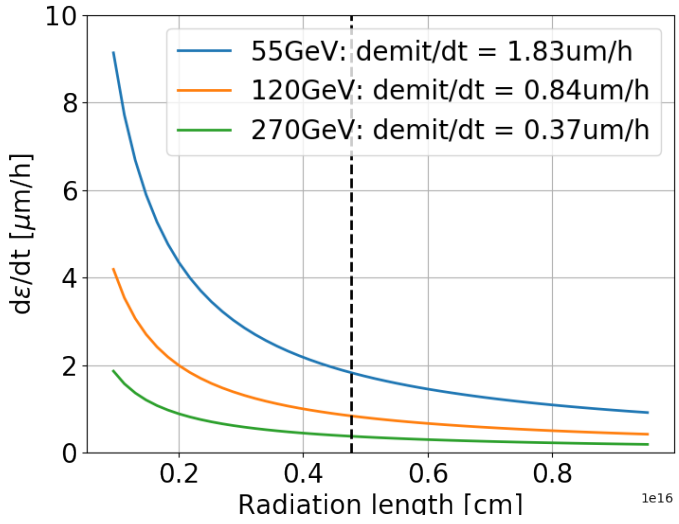

Fig. 5: Emittance growth due to residual gas scattering versus the radiation length, for three different energies.

The multiple Coulomb scattering of the proton beam with the residual gas (RGS) in the beam pipe can lead to emittance growth or beam losses [13]. An analytical parameterisation of the RGS emittance

growth with the radiation length is shown in Fig. 5. The different curves correspond to the three coast energies of the SPS for which emittance growth data are available: 55, 120, 270 GeV [1]. Vacuum decomposition measurements using a residual gas analyser were performed in the SPS in 2011 [14]. Based on those measurements, corresponding to a radiation length of $9.53{\cdot}10^{14}$ cm, the estimated emittance growth is 1.86, 4.19 and 9.14 μm/h at 270, 120, and 55 GeV respectively. Those values are much larger than the observed emittance growth in the machine for all three energies. Assuming a 5 times larger radiation length (i.e. better vacuum quality), the estimated emittance growth is 0.37, 0.83 and 1.83 μm/h respectively, which matches very well the observed emittance growth for all three energies.

1.2 After the CC installation

During the SPS tests of May-November 2018, emittance growth measurements took place during two MDs. What needed to be studied was the level at which the cavity voltage feedback provides transverse kicks to the beam at frequencies which are resonant with the beam transverse motion as this could lead to unacceptably large emittance growth over time. The two MDs were performed in coast for time scales found in the operation of the LHC. An additional signal generator (range DC to 10 kHz) was mixed with the spectrum coming from the cavity feedback in order to control the amplitude of the feedback at the first betatron sideband i.e. control the strength at which the feedback is kicking at a specific resonant frequency (see Figure 6 [15]). The results from these measurements can be found in Fig. 7. As can be seen, the measured emittance growth is consistently a factor of 2 below the predictions. This is a step in the positive direction, however more work needs to be performed in the future to understand the discrepancy.

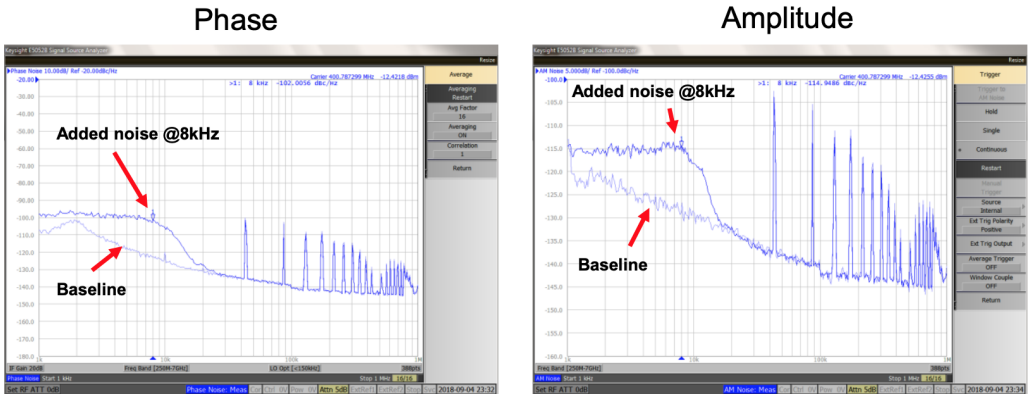

Fig. 6: Power density squared of the noise signal sent to the cavity feedback; the RF noise (phase and amplitude) covered a band from DC to 10 kHz and excited only the first betatron band ($\sim$8 kHz).

1.3 Summary of SPS emittance growth

During the SPS CC tests of 2018, only a very limited experimental time was available (seven 10 h MDs within 6 months), and during that experimental time only two MDs were dedicated to the long-term emittance growth studies. With this in mind a very good preparation prior to the CC installation was essential in order to have efficient experimental tests.

In the past few years many MDs took place in the absence of CCs to characterise the transverse natural emittance growth in the SPS and help distinguish it from the growth that would be induced during the SPS experiments through CC amplitude and phase jitter. In the absence of CCs, all MDs, apart from the last one of 2017, showed a clear dependence of the horizontal emittance growth on the chromaticity. It was also found that the intra-beam scattering mechanism can explain part of the transverse emittance growth, however, a residual growth between 0.3-0.5 μm/h was always present in both planes. This residual growth could be a result of the power supply ripple and the residual gas scattering. The first RF noise measurements on the CC module in SM18 indicated a larger low level RF (LLRF) noise than expected leading to potential emittance growth from phase noise to be between 2-8 μm/h scaled to SPS

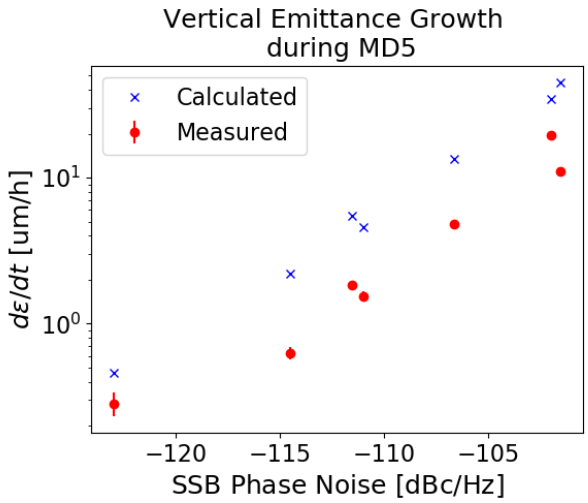

Fig. 7: Summary of emittance growth measurements as a function of the feedback noise at the frequency of the first betatron sideband.

parameters between bunch lengths of 1-2 ns [16]. This is well above the measured growth with the optimised setup during the SPS 270 GeV coasts.

After installing the CCs, two emittance growth MDs took place during the SPS tests of May-November 2018 where RF noise (phase and amplitude) was added in order to excite the first betatron band (∼8 kHz). However, the measured emittance growth was consistently found to be a factor of 2 below the predictions; studies are undergoing to understand the results.

2 Higher order CC multipoles

The tight space constraints in High Luminosity LHC (HL-LHC) [17] at the location of the CCs result in axially non-symmetric cavity designs that introduce higher order multipole CC components [18]. The impact of these higher order components on the dynamic aperture (DA) in the SPS machine, that served as a test-bed for the first CC experiments with protons (May-November 2018 [8]), is presented. Although similar findings have been reported in [6] and [19] using the multipolar values found in [18], the results provided in this report correspond to values close to the updated multipolar design values found in [20]. The results of DA studies in the presence of SPS-nonlinearities are also discussed.

2.1 CC Multipoles in a perfect SPS lattice

The DA in the SPS was studied for different CC multipole configurations, with the multipoles applied only on the first CC. Note that other than the chromatic sextupoles (for chromaticity correction), no other SPS non-linearities and no aperture constraints were included. Given that the SPS experiments were performed with different CC phase configurations, the simulations were done for a phase-cancelling mode, where $\phi_1 = 0^o$, $\phi_2 = 180^o$, and an in-phase mode: $\phi_1 = \phi_2 = 0^o$. In the first case the effect of CC kicks are cancelled out whereas in the latter they are added.

The SPS parameters at the location of the CCs are given in Table 2[1] and the used CC RF multipole values, similar to those found in [20], in Table 3. The simulations were performed for the SPS injection energy, $\mathrm{E} = 26\ \mathrm{GeV}$, as this exhibits the largest CC kick, with $\mathrm{V_{CC}} = 2\ \mathrm{MV}$, $\Delta \mathrm{p/p} = 10^{-3}$ and $\mathrm{Q'_{x,y}} = 0.0$. The indices $1, 2$ indicate the first and second CC respectively. The simulations were performed using MAD-X [22] and SixDesk [23], for 10^6 turns. Since the CCs are vertical, quadrupolar and octupolar errors are normal multipoles ($\mathrm{b}_2, \mathrm{b}_4$), whereas the sextupolar errors are skew multipoles (a_3).

[1]Note that the definition of the invariant longitudinal emittance ϵ_s in units $\mathrm{e} \cdot \mathrm{Vs}$ used at CERN is [21]: $\epsilon_s = 4\pi\sigma_t\sigma_{\frac{\Delta E}{E_0}} E_0$, where σ_t is the rms bunch length in seconds and $\sigma_{\frac{\Delta E}{E_0}}$ is the relative rms energy spread; the bunch length is usually quoted as 4σ value, $\tau \equiv 4\sigma$.

Table 2: Parameter table

Parameter	**Value**
nCavities	2
s-location [m]	6312.7213, 6313.3213
Transverse tilt [deg]	90
f [MHz]	400.528
$\beta_{\mathrm{x1}}, \beta_{\mathrm{y1}}$ [m]	29.24, 76.07
$\beta_{\mathrm{x2}}, \beta_{\mathrm{y2}}$ [m]	30.31, 73.82
$\mathrm{Q_x}, \mathrm{Q_y}$	26 .13, 26.28
$\mathrm{E_{inj}}$ [GeV]	26.00
γ_{rel}	27.71
$\epsilon_{n,x}, \epsilon_{n,y}$ [$\mu\mathrm{m} \cdot \mathrm{rad}$]	2.50, 2.50
$\mathrm{V_{RF}}$ [MV]	2
$\Delta\mathrm{p/p}$	10^{-3}
Bunch length [m] (1σ)	0.23
ϵ_{s} [$\mathrm{eV} \cdot \mathrm{s}$] (see footnote for definition)	0.5

Table 3: Values of CC multipoles (DQW) used in this report, in units of $\mathrm{mTm/m^{n-1}}$ at nominal deflecting voltage V_{CC}=10 MV, similar to what can be found in [20]

Multipole	**Value**
$\mathrm{b_2}$ (Q)	6
$\mathrm{a_3}$ (S)	1506
$\mathrm{b_4}$ (O)	2106

The DA with respect to angle for the studies described above are shown in Fig. 8 for the cases where the CCs are in a phase-cancelling (top) or in-phase (bottom) mode respectively. In both plots the dashed horizontal line is the physical aperture, 7.6σ, when no CCs are present. In Fig. 8 (top) it can be seen that, as expected, there is a complete overlap between the cases in the absence and presence of phase-cancelling CCs, both in the absence of CC multipoles (black and orange lines respectively; note that the black line is behind the orange one). When the multipoles are added one at a time the DA reduces mainly when the sextupolar multipole is present on its own (green line) or in combination with the other multipoles (purple line); even then though, the DA is as high as $\sim 40\sigma$. Note that, as mentioned above, the multipoles were applied only on the first CC so that we could study the multipole effect when using the CCs in a phase-cancelling mode; otherwise, if the multipoles were applied to both CCs their effect would be cancelled out.

On the other hand, when the CCs are in-phase (bottom plot of Fig. 8) the DA reduction is dominated by the cavities themselves, and not by the CC multipoles; this is clear from the fact that the orange line (CCs present, without CC multipoles) overlaps with all other coloured lines that include CC multipoles. In other words these simulations showed that the DA in the presence of the CC and CC multipoles, when used with the design values, remains significantly larger than the physical aperture and therefore no effect on lifetime, halo etc is expected to be observed.

2.1.1 Minimum Dynamic Aperture for different multipolar strengths

Additional studies took place calculating the minimum DA for a large range of the multipolar strength values, for an initial momentum deviation of $\Delta\mathrm{p/p_{init}} = 10^{-3}$ and for in-phase CCs ($\phi_1 = \phi_2 = 0^{\mathrm{o}}$) set to 2 MV each. Figure 9 shows the minimum DA for $\mathrm{b_2}$ (top), $\mathrm{a_3}$ (middle) and $\mathrm{b_4}$ (bottom) values that range from 0 to values that are two or three order of magnitudes larger than the design values (black vertical line); the dashed horizontal line shows the physical aperture of 7.6σ.

As expected, the stronger the multipolar value the smaller the DA. In the $\mathrm{b_2}$ and $\mathrm{a_3}$ cases the DA becomes smaller than the physical aperture at values that are three or two orders of magnitude larger than

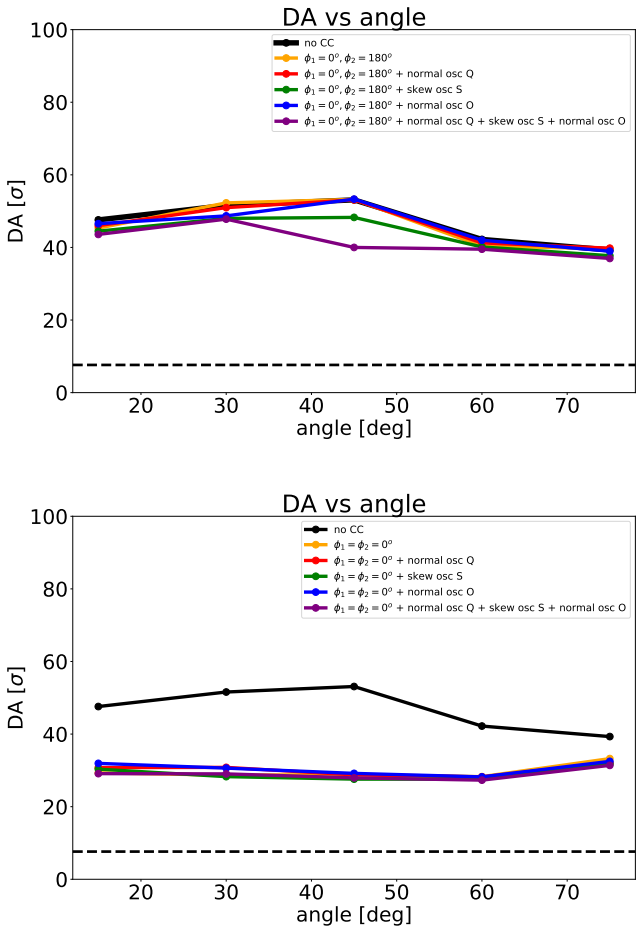

Fig. 8: DA in σ with respect to angle in transverse phase space when the CCs are in a phase-cancelling mode (top), i.e. $\phi_1 = 0^o$ and $\phi_2 = 180^o$, or an in-phase mode (bottom), i.e. $\phi_{1,2} = 0^o$; Q: quadrupolar, S: sextupolar, O: octupolar multipoles. The dashed horizontal line is the physical aperture when no CCs are present (7.6σ).

the design values, respectively; in the b_4 case we are limited from the physical aperture, and not by DA, even for values that are three orders of magnitude larger than the design values. During the SPS tests of May-November 2018, an experimental effort took place to characterise with two different techniques the CC a_3 component [7].

2.2 DA in the presence of SPS non-linearities

The aforementioned results do not include any non-linear fields other than the chromatic sextupoles used for chromaticity correction. The realistic SPS model though includes other sources of non-linearities among which the most important ones are the odd multipoles produced by the error harmonics of the main dipole magnets and remanent fields in sextupoles and octupoles due to magnetic hysteresis; the latter relevant only at low energies.

In order to establish the SPS non-linear optics model with beam-based measurements at injection energy (26 GeV) [24], chromaticity measurements were repeated (see Figure 10) for 3 different optics (Q20, Q22, Q26, where the integer part of tune is 20, 22 and 26 and the non-integer part is 0.13 and 0.18 in the H and V plane respectively), exhibiting different betatron and dispersion functions; in this way the contribution of the different non-linear errors was disentangled. An effective optics model has been built by fitting the strength of the multipolar errors in order to reproduce the experimental observations with the 3 different optics. The procedure has been repeated 5 times for different machine configurations, allowing to establish an average model and to evaluate the statistical uncertainties. While the majority of the SPS CC tests have been carried out at the injection energy of 26 GeV, a beam energy of 270 GeV

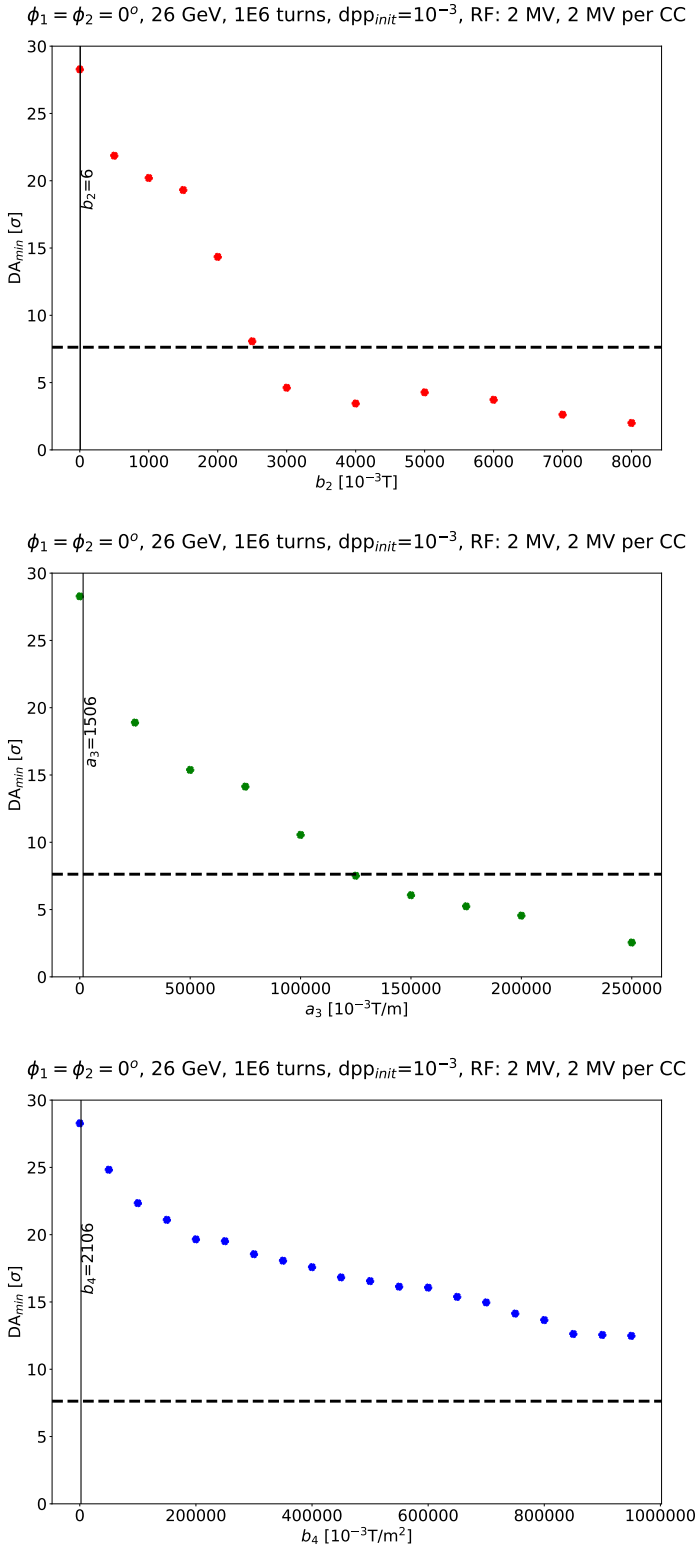

Fig. 9: Minimum DA in σ with respect to b_2, a_3 and b_4; the vertical black line shows the multipolear design value and the dashed horizontal line the physical aperture of 7.6σ.

was employed in some measurements. To confirm the validity of the effective non-linear model at higher energy, a single chromaticity measurement of the Q26 optics at 270 GeV was acquired and used to fit a model containing the odd multipoles produced by dipoles only. Independent parameters for each multipolar error have been allowed for each of the two different kinds of SPS dipoles, MBA and MBB, that have different aperture but same length and integrated field.

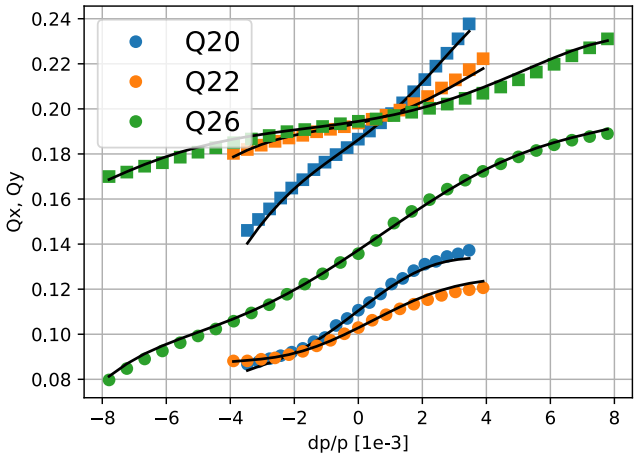

Fig. 10: Horizontal (dots) and vertical (square) fractional tune measured during a typical momentum scan for Q20, Q22 and Q26. Because of the different dispersion values in the 3 optics, the $\mathrm{dp/p}$ range has been adjusted in order to cover the same radial excursion. The chromaticity computed from the effective model obtained from the fit of the 3 measurements is also shown (black curves).

Table 4: Multipole errors from SPS nonlinear model

Multipole	26 GeV	270 GeV
$\mathrm{b_{3a}}[m^{-2}]$	$(-2.8 \pm 0.6) \cdot 10^{-3}$	$8.1 \cdot 10^{-4}$
$\mathrm{b_{3b}}[m^{-2}]$	$(1.6 \pm 0.3) \cdot 10^{-3}$	$1.1 \cdot 10^{-3}$
$\mathrm{b_{5a}}[m^{-4}]$	-7.9 ± 0.5	9.2
$\mathrm{b_{5b}}[m^{-4}]$	-6.8 ± 1.5	-10
$\mathrm{b_{7a}}[m^{-6}]$	$(8.8 \pm 2.6) \cdot 10^{4}$	$1.3 \cdot 10^{5}$
$\mathrm{b_{7b}}[m^{-6}]$	$(1.7 \pm 0.8) \cdot 10^{5}$	$1.4 \cdot 10^{5}$

Table 4 shows a comparison of the simplified model measured at 270 GeV against what was measured at injection energy [24]. The two models are found to be compatible, except for the sextupolar component of the MBA dipoles ($\mathrm{b_{3a}}$). However such a discrepancy is likely to be attributed to a calibration error of the sextupoles used to correct chromaticity. The overall good agreement extends the validity of the effective model measured at injection energy to the conditions used for the CC simulations.

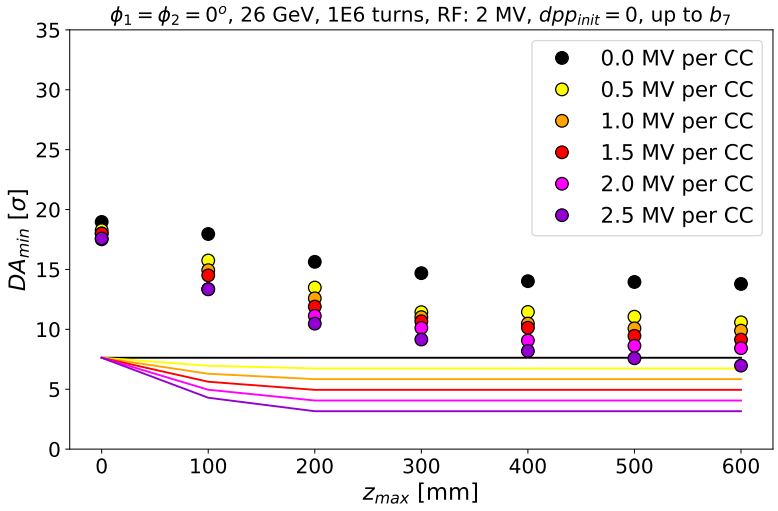

Fig. 11: Minimum DA for different initial longitudinal actions, z, and CC voltage; the physical aperture is shown by the horizontal lines

Due to the synchrotron oscillations, a particle with a specific initial $\Delta p/p$ or longitudinal action, z, will see a variation of the CC field; the larger the initial longitudinal action is, the larger the range of the CC wavelength the particle will experience. To study the effect this has on DA the following simulation was performed for $\Delta p/p_{init} = 0$ but with different initial z, and was repeated for voltages ranging from 0 to 2.5 MV per CC (Fig. 11). These simulations did not include the CC multipoles, as it was shown they have no effect on DA for the design multipolar values, but instead took into account the non-linear SPS fields, up to b_7. The study was performed for 10^6 turns with the CCs being in-phase ($\phi_1 = \phi_2 = 0^o$). The horizontal lines of Fig. 11 represent the SPS physical aperture. These simulations demonstrate a very positive result: even for the largest z and the highest operational voltage of 2.5 MV per CC, the particles are only limited by the physical aperture that drops from 7.6σ to 3.2σ, and not by DA.

2.3 RF Multipolar Components (a_3) measurement

The non-linearity of the 400 MHz fundamental mode of the CC can give rise to higher order multipole components that can affect the beam dynamics in the machine (for example by reducing the dynamic aperture). These are of particular concern (as compared with static multipolar components) as they cannot be corrected due to the dependence on cavity parameters. Of primary concern with this particular CC model (DQW) is the skew sextupolar (a_3) component.

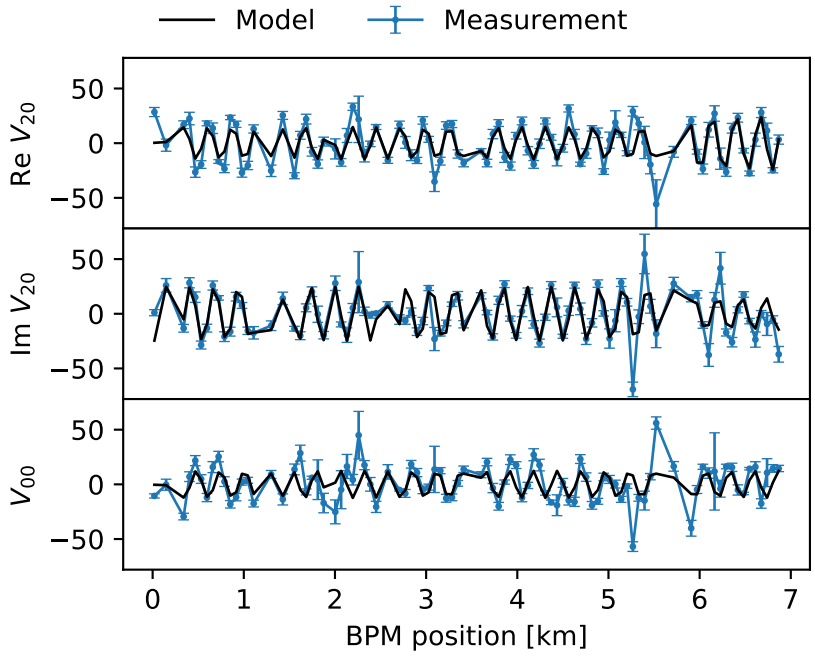

Fig. 12: Real and imaginary components of the V20 resonance line for +1MV in the cavity (at 90° crabbing phase) and -1 MV in the cavity (or +1 MV with 270° crabbing phase). The analytical model has been scaled in order to fit the measured data and determines the strength of a_3. Furthermore a phase of ∼40° was introduced to match the V20 model to the measurements suggesting that the measurement could be spoiled by some other source of a_3.

During the SPS CC tests, the a_3 was measured by kicking in the horizontal plane and measuring the vertical betatron motion driven by the skew sextupolar field. The vertical motion was thus decomposed in two main contributors: the spectral line V20, whose frequency is 2 times the horizontal tune, and the spectral line V00, whose frequency is 0 [7]. The amplitude of V20 and V00 depends linearly on a_3, the horizontal action and a term depending on the optics. Therefore by comparing the turn-by-turn observation of the V20 and V00 spectral lines obtained from the BPMs, and an analytical model obtained from the first order perturbative theory it was possible to derive the value of a_3.

It can be seen that while the trends of the measured spectral lines V00 and V20 follow correctly the analytical model, a strong disagreement in terms of overall phase of the V20 spectral line is present. Such disagreement can be ascribed to the presence of non-linearities in the SPS optics that, along with

the large vertical orbit produced by the CC, can affect by a feed-down effect the V00 and V20 spectral lines. A deep understanding of the SPS non-linear model is therefore necessary and an effort to work out the required details is being carried out.

2.4 Summary of CC and SPS higher order multipoles simulations and measurements

The simulation results of the SPS DA studies for CCs in the presence of CC multipoles and machine non-linearities showed that the CC multipoles play no significant role in the DA for the design values. In order to see an important effect for the b_2 and a_3 cases, multipoles that are three and two orders of magnitude larger than the design values respectively need to be employed, whereas in the b_4 case even for values that are three order of magnitudes larger we are still limited by the physical aperture and not by DA. Finally, it was shown that in the presence of machine non-linearities (up to b_7) our beam is only limited by the physical aperture, and not by DA, even for high CC voltages and large initial longitudinal actions. During the SPS tests a measurement of the a_3 component has been attempted. However more work is required to fully disentangle the a_3 contribution of the crab-cavity from other optics-related effects.

3 Instrumentation observations during the SPS CC experiments

The world's first injection of a proton beam into a CC occurred on the 23^{rd} of May 2018 at 12:55. Shortly afterwards, the synchronisation between the SPS and the CC RF signal was setup and optimised and regular synchronous crabbing was observed. Figure 13 shows a reconstruction of the crabbing motion taken from the head-tail (HT) monitor.

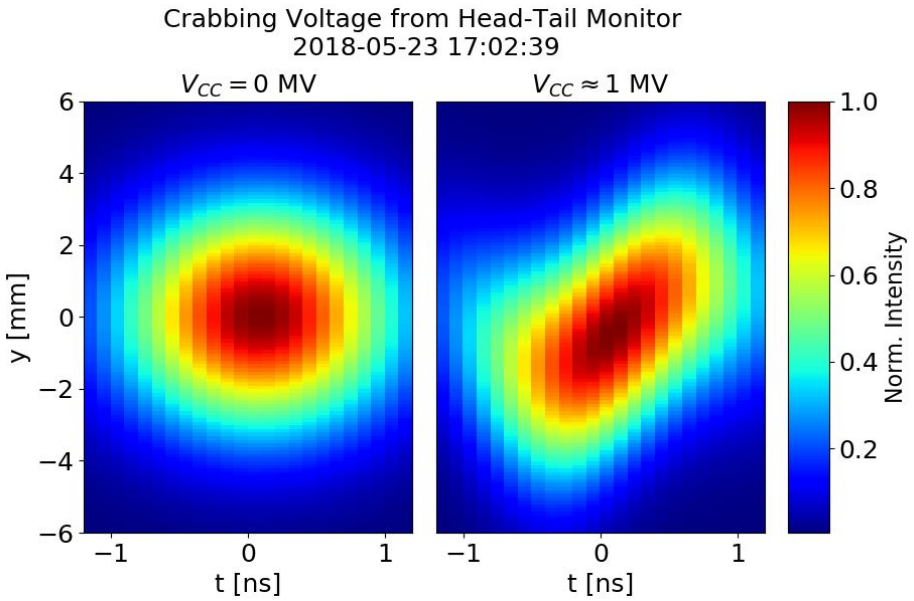

Fig. 13: CCs off (left) and on (right).

3.1 Crab dispersion

As explained in [25] the effect a CC has on a particle is like the one of an orbit corrector, or dipole, with the only difference being that the crab kick is z-dependent. Following the closed-orbit distortion approach, one can get the deviation of the crab closed orbit with a specific longitudinal position along the bunch:

$$\mathrm{x_{D_{CC}}(z,s)} = \sqrt{\beta(\mathrm{s_0})\beta(\mathrm{s})}\frac{\theta}{2\mathrm{sin}\pi\mathrm{Q}}\mathrm{cos}\big(\psi(\mathrm{s},\mathrm{s_0}) - \pi\mathrm{Q}\big) \tag{1}$$

where θ is the dipolar (or CC) kick, z the longitudinal position of the particle in the bunch (with respect to the bunch centre), $\beta(s)$ and $\beta(s_0)$ are the beta functions along s and at the CC-location respectively,

$\psi(s, s_0)$ is the phase advance between the CC and the s-location in the ring, and Q is the tune. The "crab dispersion" is defined as the orbit deviation at $z = 1\sigma_z$ normalised to $1\sigma_P$:

$$D_{CC}(s) = \frac{x_{D_{CC}}(1\sigma_z, s)}{1\sigma_P}. \tag{2}$$

Some fundamental checks were made to compare the orbit response of the beam with simulations. This was of particular interest as it was not clear how the BPMs would respond to a crabbing bunch. Figure 14 shows the measured CC orbit distortion compared with the MAD-X optimisation.

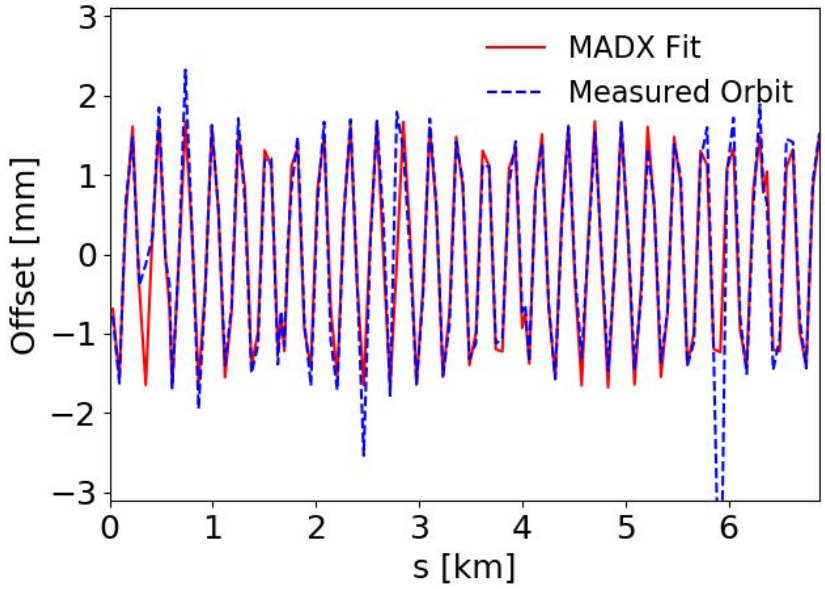

Fig. 14: Comparison of CC closed orbit with MAD-X fit.

It was found that while the phase behaviour was in good agreement with the model for the SPS produced by MAD-X, the equivalent voltage needed to reproduce the behaviour was approximately a factor of 2 lower than what the other CC diagnostics were showing; i.e. the power sensors were measuring 1 MV, the HT monitor 1.2 MV (this value was provided using data coming from the calibration of the instrument), but the BPM response was showing 0.7 MV.

Upon closer inspection, it was found that difference has to be attributed to the characteristic spectral response of the BPM. The effective beam position measured by BPM, whose spectral response follows the distribution $R(\omega)$ is obtained as:

$$\bar{X} = \frac{|R(\omega) \cdot \mathcal{F}\{I(t) \cdot X(t)\}|}{|R(\omega) \cdot \mathcal{F}\{I(t)\}|} \tag{3}$$

where, $I(t)$ is the bunch longitudinal distribution, $X(t)$ is the bunch transverse position (averaged over the transverse distribution) and $\mathcal{F}$ represents the Fourier transform operator. In the case of the Multi Orbit POsition System (MOPOS) BPMs installed in the SPS, $R(\omega)$ reduces to a δ distribution centred around 200 MHz. Figure 15 shows the measured beam position by a MOPOS BPM normalised by the actual peak orbit (or the orbit produced by a static field whose strength is equal to the peak CC field) as a function of the bunch length, assuming a gaussian longitudinal distribution.

Applying the proper correction to the CC closed orbit measurement shown in Fig. 14, where a 4σ bunch length of 2.9 ns was observed, increases the estimated CC voltage to 1.34 MV, a value considered within the uncertainty of the RF measurement.
The BPMs used in the LHC instead employ a wide bandwidth electronic and more work is still required in order to ascertain the exact shape of the frequency response.

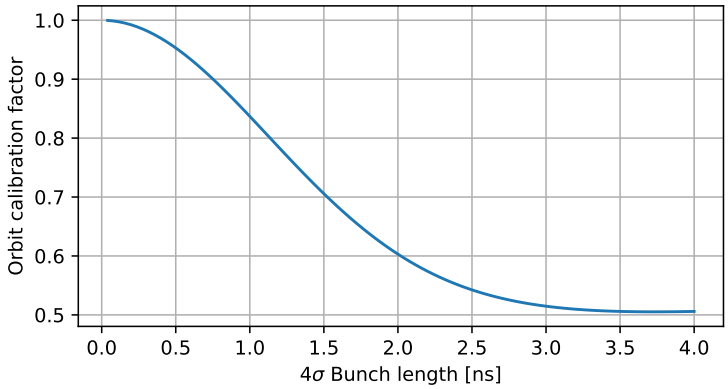

Fig. 15: Response of a MOPOS BPM obtained from Eq. 3 as a function of the bunch length in the case of a longitudinal bunch distribution and assuming the beam on crest with respect to the CC field

3.2 Cavity transparency

A constant question surrounding operation of the CCs in the LHC was whether or not they can be "switched off" in the event of issues with the cavities, i.e. can the cavities be counter phased such that the total crabbing that the beam sees is zero. During the last MD, with 1 MV in each cavity, the phases were optimised such that a total crabbing voltage of 60 kV was observed. Note that the 60 kV value was not obtained from a careful fitting of the full sinusoidal response but instead was taken from the online measurements during the MD as the best compensation. It can be seen clearly in Figure 16 that the beam response was minimal in transparent mode in both simulations (top) and measurement (bottom).

3.3 Summary SPS CC instrumental observations

The SPS HT monitor and BPMs were used to measure the world's first crabbing of a proton beam during the SPS tests in 2018. The results of these tests will be used to update the design of the HL- LHC CCs and lessons learnt from these tests will help plan future CC tests in the SPS.

4 References

[1] R. Calaga, L. Ficcadenti, E. Metral, R. Tomas, J. Tuckmantel, and F. Zimmermann. Proton-Beam Emittance Growth in SPS Coasts. *Conf. Proc.*, C1205201:3737–3739, 2012.

[2] F. Antoniou, A. Alekou, H. Bartosik, T. Bohl, R. Calaga, L. Carver, J. Repond, and G. Vandoni. Emittance growth in coast in the SPS at CERN. page MOPMF061, 2018. [J. Phys. Conf. Ser.1067,no.2,022008(2018)].

[3] A. Alekou, F. Antoniou, R. Appleby, G. Arduini, H. Bartosik, R. Calaga, Y. Papaphilippou, and C. Welsch. SPS Studies in Preparation for the Crab Cavity Experiment. In *Proceedings, 8th International Particle Accelerator Conference (IPAC 2017): Copenhagen, Denmark, May 14-19, 2017*, page TUPVA034, 2017.

[4] A. Alekou, F. Antoniou, H. Bartosik, and R. Calaga. Emittance growth in coast in the SPS. In *Proceedings, Injector MD Days 2017: CERN. Geneva, Switzerland, March 23?24, 2017*, pages 107–112, 2017.

[5] P. Baudrenghien and T. Mastoridis. Transverse emittance growth due to rf noise in the high-luminosity LHC crab cavities. *Phys. Rev. ST Accel. Beams*, 18(10):101001, 2015.

[6] A. Alekou et al. Beam dynamics simulations with crab cavities in the SPS machine. MOPGW095, IPAC 2019.

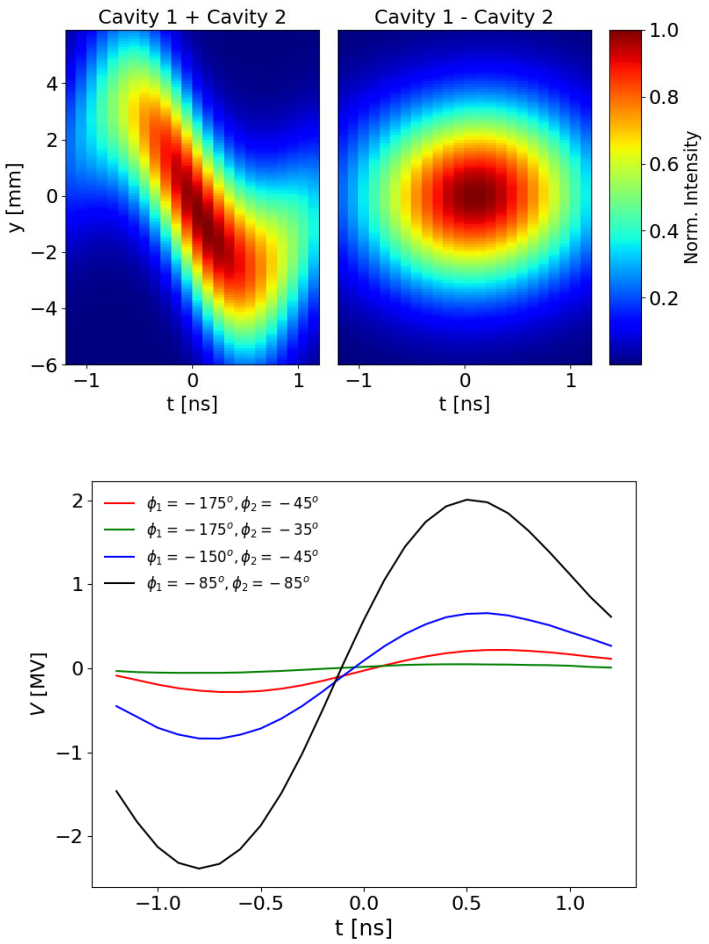

Fig. 16: Top: Simulation of cavities in an in-phase (left) and counter-phase modes (right) with 1 MV in each cavity. Bottom: HT monitor measurement; the green line corresponds to the phase where the transparency was achieved.

[7] M. Carla' et al. Beam-based measurement of the skew-sextupolar component of the radio frequency field of a hl-lhc-type crab-cavity. MOPTS090, IPAC 2019.

[8] L. R. Carver et al. Beam dynamics results with crab cavities in the super proton synchrotron. MOPGW094, IPAC 2019.

[9] Federico Roncarolo. Accuracy of the Transverse Emittance Measurements of the CERN Large Hadron Collider, 2005. Presented 2005.

[10] A. Piwinski. Intra-beam-Scattering. In *Proceedings, 9th International Conference on the High-Energy Accelerators (HEACC 1974): Stanford, California, May 2-7, 1974*, pages 405–409, 1974.

[11] F Antoniou and F Zimmermann. Revision of Intrabeam Scattering with Non-Ultrarelativistic Corrections and Vertical Dispersion for MAD-X. Technical Report CERN-ATS-2012-066, CERN, Geneva, May 2012.

[12] Y. Papaphilippou et al. Operational Performance of the LHC Proton Beams with the SPS Low Transition Energy Optics. In *Proceedings, 4th International Particle Accelerator Conference (IPAC 2013): Shanghai, China, May 12-17, 2013*, page THPWO080, 2013.

[13] Dugan G. USPAS lectures on Beam loss and beam emittance growth. 2002.

[14] Kim H J and Sen T. Beam simulation of the SPS. 2011.

[15] L. Carver. First proton beam dynamics results with crab cavities. Available at `https://indico.cern.ch/event/800428/attachments/1804664/2945632/CrabCavity_BE_Seminar.pdf`, 2019.

[16] Baudrenghien P. and Mastoridis T. Private communication.

[17] Apollinari G. and Bèjar Alonso I. and Brüning O. and Fessia P. and Lamont M. and Rossi L. and

Tavian L. *High-Luminosity Large Hadron Collider (HL-LHC): Technical Design Report V. 0.1*. CERN Yellow Reports: Monographs. CERN, Geneva, 2017.

[18] J. Barranco Garcìa, R. De Maria, A. Grudiev, R. Tomàs Garcìa, R. B. Appleby, and D. R. Brett. Long term dynamics of the high luminosity Large Hadron Collider with crab cavities. *Phys. Rev. Accel. Beams*, 19(10):101003, 2016.

[19] A. Alekou, R. Appleby, H. Bartosik, R. Calaga, M. Carla', and Y. Papaphilippou. SPS Long Term Stability Studies in the Presence of Crab Cavities and High Order Multipoles. In *Proceedings, 61st ICFA Advanced Beam Dynamics Workshop on High-Intensity and High-Brightness Hadron Beams (HB2018): Daejeon, Korea, June 17-22, 2018*, page WEP2PO008, 2018.

[20] R. Calaga and J. Mitchell. Latest info on field quality for crab cavities. Available at `https://indico.cern.ch/event/826475/contributions/3457534/attachments/1872608/3082026/WP2_Multipole_Update.pdf`, 2019.

[21] Oliver Sim Brüning, Paul Collier, P Lebrun, Stephen Myers, Ranko Ostojic, John Poole, and Paul Proudlock. *LHC Design Report*. CERN Yellow Reports: Monographs. CERN, Geneva, 2004.

[22] L. Deniau; H. Grote; G. Roy; F. Schmidt and many other contributors. MADX. Available at `http://mad.web.cern.ch/mad/`.

[23] E. McIntosh and R. De Maria. Sixtrack - 6d tracking code. `http://sixtrack-ng.web.cern.ch/SixTrack/doc/sixdesk/sixdesk$\_$env.html`.

[24] M. Carla', H. Bartosik, M. Beck, K. Li, and M. Schenk. Studies of a New Optics With Intermediate Transition Energy as Alternative for High Intensity LHC Beams in the CERN SPS. In *Proceedings, 9th International Particle Accelerator Conference (IPAC 2018): Vancouver, BC Canada, April 29-May 4, 2018*, page TUPAF022, 2018.

[25] Yi-Peng Sun, Ralph Assmann, Javier Barranco, Rogelio Tomas, Thomas Weiler, Frank Zimmermann, Rama Calaga, and Akio Morita. Beam dynamics aspects of crab cavities in the CERN Large Hadron Collider. *Phys. Rev. ST Accel. Beams*, 12:101002, 2009.